Hybridization in three dimensions: a novel route towards plasmonic metamolecules

Supporting Information

Pierfrancesco Zilio[1], Mario Malerba[1], Andrea Toma[1], Remo Proietti Zaccaria[1], Andrea Jacassi[1,2] and Francesco De Angelis[1*]

[1]Istituto Italiano di Tecnologia, Via Morego 30, 16163 Genova, Italy

[2]Università degli studi di Genova, Via Balbi 5, 16126 Genova, Italy

[*]AUTHOR EMAIL ADDRESS: francesco.deangelis@iit.it

Contents

1. Fabrication of slanted nanorod dimers arrays

Extruding structures with extremely high-aspect-ratio can be obtained in vertical or tilted configurations (such as needles, cones, nano-fences, nanotubes etc.) by means of secondary electron lithography. A thorough discussion of the technique is reported in ref. [42] in the main text.

A 100nm thick silicon nitride membrane is used as support, and s1813 optical resist is spin-coated and soft-baked on the flat top-side. The s1813 layer thickness determines the final height of the rods. A focused ion-beam (Helios Nanolab 600, FEI company) is used to pattern the sample from the backside (namely from the silicon nitride side), tilting the stage to provide the required slant angle α (30° with respect to the normal, see Figure 1a in the main text). Processing the device from the backside guarantees clean and straight nanotubes, whereas a direct milling on the resist from the top-side would produce funnel-like structures and dangling polymer residues. The two rods constituting the dimers are obtained by two separate patterning steps, the second one performed after rotating the specimen by β = 90° degrees. Since the patterning takes place from the base of the structures, a precise positioning of every line of rods becomes mandatory to guarantee a precise nanometric gap at the end of the tubes, thus taking into precise account polymer thickness, tilt angle and array pitch after rotation. Once the specimen is patterned on a range of different gap sizes and pitch values, it is developed with acetone and rinsed in isopropyl alcohol; the last step and the drying of the sample is performed in a supercritical CO_2 atmosphere, to avoid collapse into no-gap layouts. A mild oxygen plasma treatment at last thins the residual resist skin from 40 nm down to 10 nm, producing homogeneous and smooth sides, which are at last used as scaffolds, sputter-coated with 30 nm of silver and annealed in N_2 atmosphere. Scanning Electron microscope images of examples of the fabricated structures are reported in Figure S1. The final structures consist of hollow metal nanotubes, with a diameter of 160nm and silver wall thickness of 30nm, while their length can range from hundreds of nanometers to several microns. We notice that a hollow core is inherently present owing to the fabrication process. While this feature may enable light transmission at VIS

wavelengths, it does not affect the optical properties of the structures at IR wavelengths, since they are much larger than the fundamental guided mode cutoff and the skin depth of silver at these wavelengths is just few nanometers.

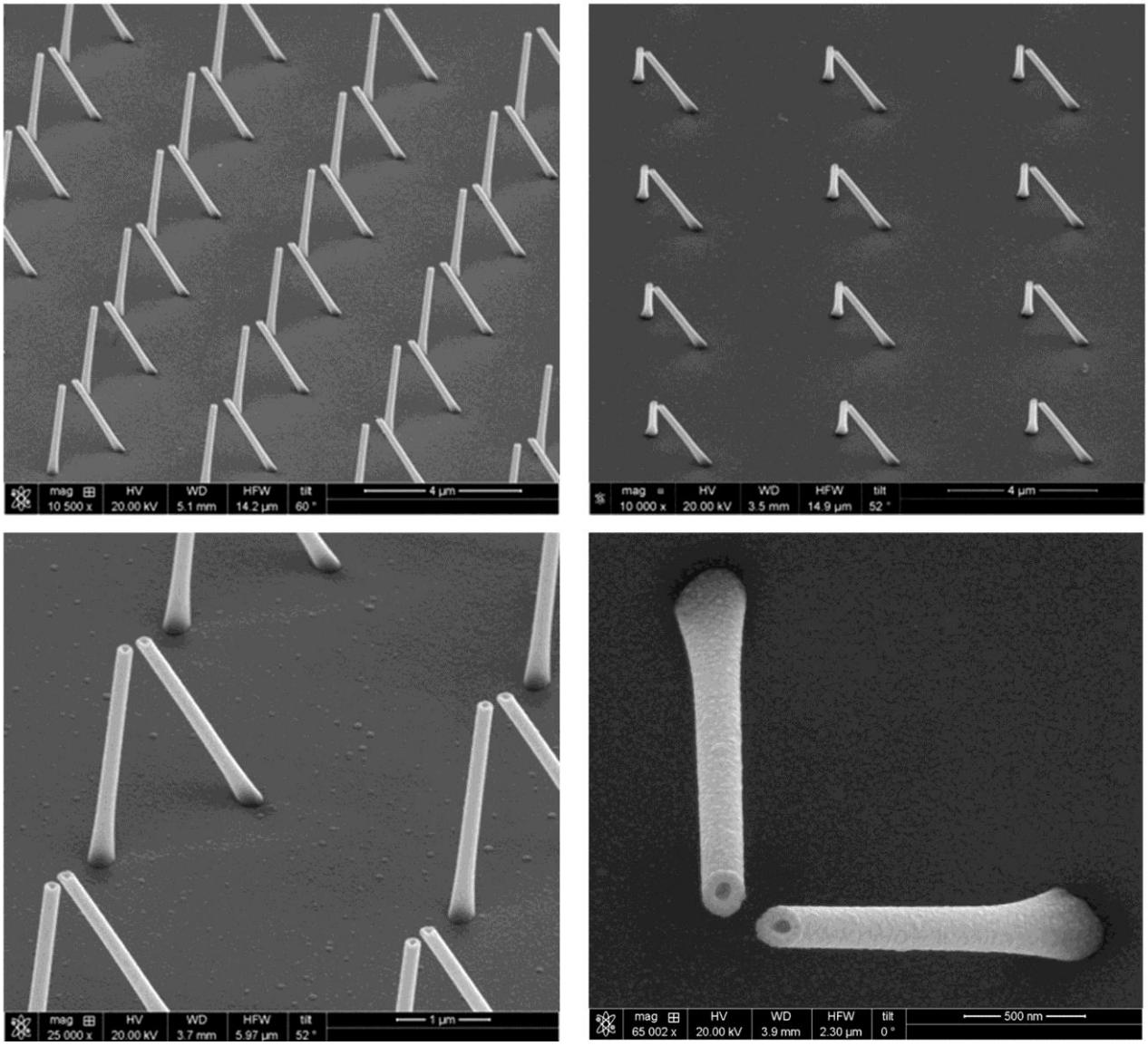

Figure S1. Scanning Electron Microscopy images of examples of fabricated nanorod dimers.

2. Effect of rounded edges on the simulation results.

The fabricated structures have rounded corners and edges (curvature radii are estimated to be around 10 nm). This has been neglected in FEM simulations in order to reduce the computational cost. The

effects on the electric field enhancement, on the resonance quality factors and on the agreement between simulations and experiment are shown in Figure S2.

As shown in Figure S2a we considered a 10nm curvature radius at the nanorods edges. As can be seen from the mesh plot, a strongly refined mesh is required to resolve this curvature, which in general determines much higher computation times. A comparison between the calculated electric field with and without fillet of the edges is reported in Figure S2b. Geometrical parameters and illumination are the same as for the simulation reported in Figure 3b of the main text. It shows no significant quantitative or qualitative differences in the electric field norm patterns and values (the maximum predicted electric field is of the same order of magnitude).

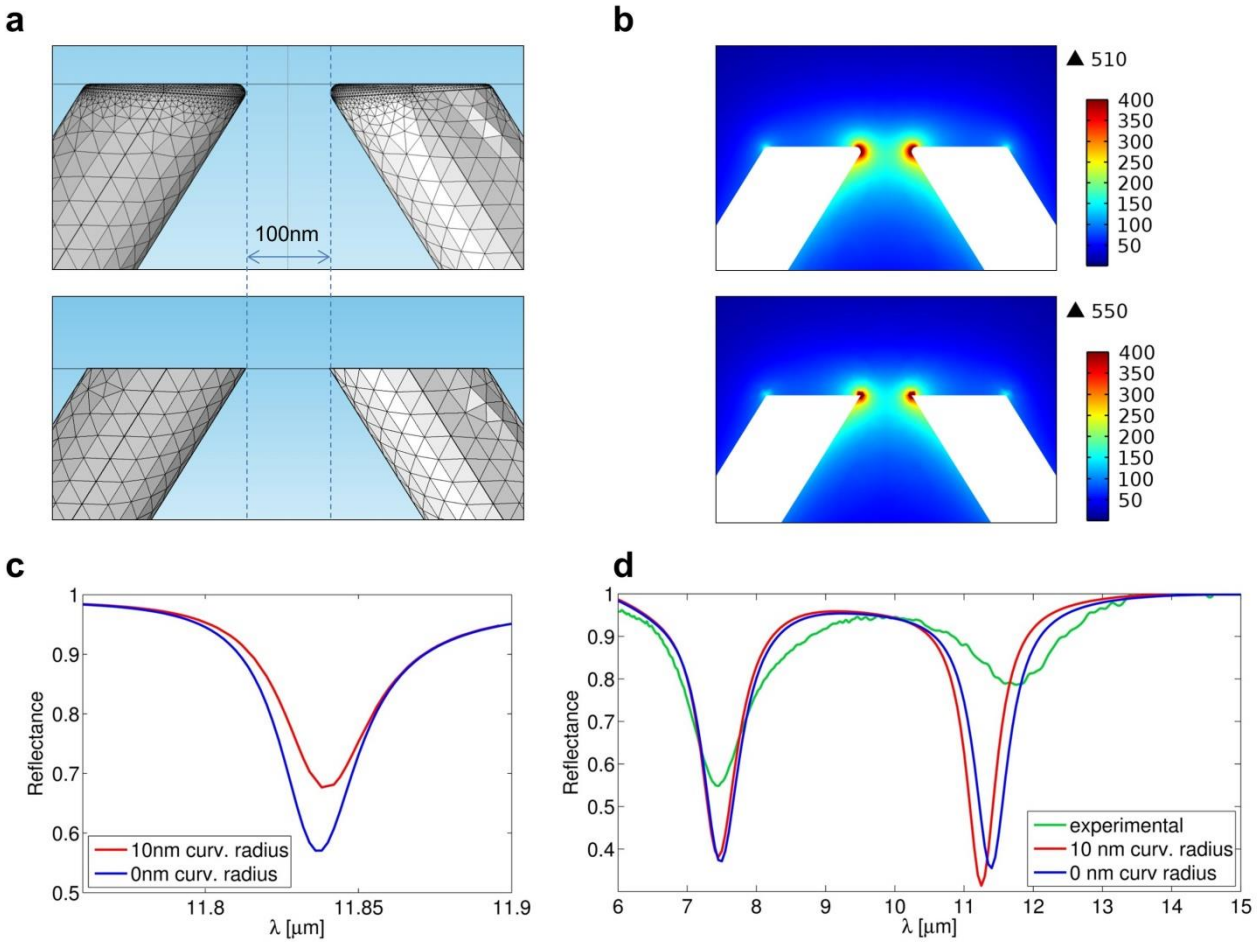

Figure S2. (a) Comparison of a mesh taking into account a 10nm edge curvature radius with a mesh neglecting it (zero curvature radius); (b) example of calculated electric fields adopting the two meshes in (a); (c, d) comparison of reflectances with the two meshes in (a) for two slanted rods geometries, the green line shows the experimental reflectance. Details of the geometrical parameters are reported in the text.

In Figure S2c we report a comparison between reflectance spectra of slanted nanorod dimers arrays with pitch optimized to obtain a high quality factor collective resonance (pitch = 8.25 μm, see Figure S4 in Supporting Information 4). The quality factor calculated without rounded edge is 389, while with rounded edge it turns out to be 351, thus remaining comparable in order of magnitude.

Finally we consider effect of the rounded edges on the agreement between simulations and experiment. In Figure S2d we plot the simulated and experimental reflectance spectra reported respectively in Figure 4d and 4f in the main text relative to the case of pitch equal to 4 μm together with the same spectrum calculated with rounded edges (red curve). As can be seen, no significant improvement of the agreement is obtained. As mentioned in the main text, the mismatch between simulations and experiment is mainly ascribable to the non-perfect control of the gap size within an antenna array and to the limitations of the experimental setup available to us, which does not allow illuminating the sample with a highly collimated light beam.

From these results we see that the rounding of the corners does not significantly improve or modify the results and conclusions drawn in the manuscript.

3. Role of the β angle in the optical properties of the slanted rods dimers.

The angle α and β defining the spatial arrangement of the slanted nanorod dimers considered in this work are shown in Figure 1 in the main text. In Figure 2c we have shown the effect of a non-zero tilt angle α on the scattering cross sections of slanted dimers, having fixed the aperture angle $\beta = 90°$ between the slanted rods. For the sake of completeness, we show here the effect of a variation of the β angle, while keeping the angle α fixed to 30°.

In Figure S3a and S3b we report respectively the normalized scattering and absorption cross section spectra with increasing of the angle $\beta' = \beta/2$ (as indicated in the figure inset) for TM (blue) and TE (red) linearly polarized plane waves impinging at an angle of 25°, with wave vector parallel to the symmetry axis of the dimer (see inset). All of the geometrical parameters of the dimer are the

same as reported in the caption of Figure 1 in the main text (namely: rods height of 1.8 μm, 100 nm gap width, 80 nm rod outer radius). The case β = 0°, in particular, corresponds to parallel slanted nanorods spaced by a distance equal to the gap width (100 nm).

As can be seen from the plots, the spectra for TM polarization show only a little dependence on the angle β. In particular, the main broad peak visible in the scattering cross section at around λ = 10 μm, corresponding to the antibonding resonance (see main text for details), is only slightly affected.

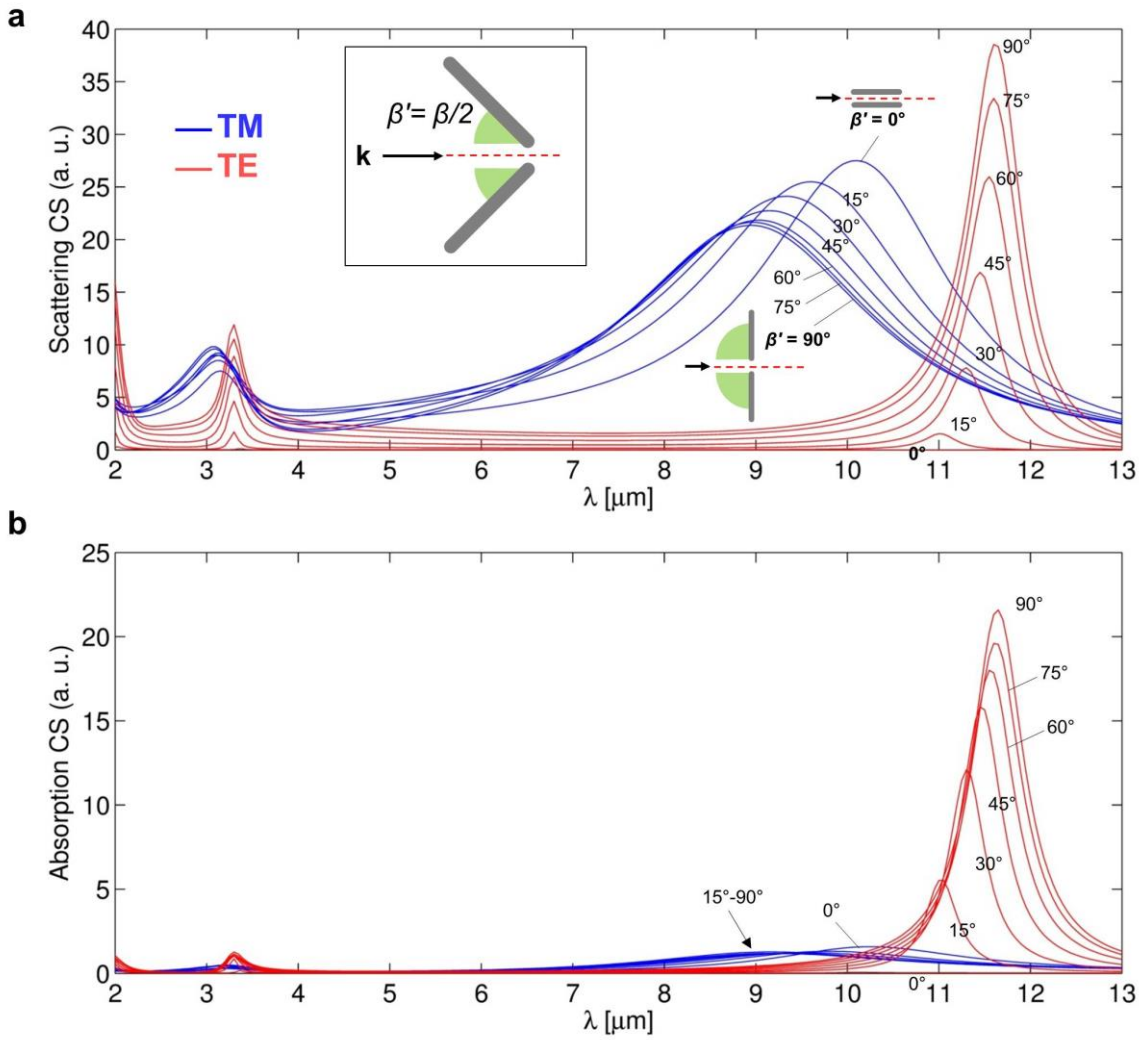

Figure S3. (a) Scattering and (b) Absorption cross sections of an isolated slanted dimers for different values of the aperture angle $\beta' = \beta/2$ (see inset). The considered scattering plane is depicted in the inset, the impinging angle being 25°. TM and TE polarizations are considered (blue and red lines respectively). The geometrical parameters of the dimers are the same as in Figure 1 of the main text.

Indeed, in this case, the projection of the geometry along the polarization direction is almost constant. By contrast, for TE polarization the projection strongly increases with β, thus enabling a dramatic increase of the coupling efficiency to the resonances of the structure (in particular, the bonding mode, extensively described in the text, is observed at around $\lambda = 11.5$ μm).

4. High-quality-factor lattice resonances optimization.

Upon a proper tuning of the geometrical parameters, it is possible to achieve high-quality-factor collective resonances for the slanted nanorod dimer arrays. As described in the main text, the dimer antibonding resonance provides high inter-dimer coupling efficiency, which results in enhanced collective resonances. By contrast the bonding resonance has an inherent local intra-dimer character and shows a weak inter-dimer interaction. In order to maximize the collective response of the array we consider the array layout and illumination depicted in Figure S4a, inset.

We consider the same slanted dimer geometrical parameters as in Figure 1 in the main text, they are listed here again in the caption of Figure S4 for convenience. Figure S4a reports the Reflectance spectra for different array pitches. As can be seen by increasing the array pitch from 5μm to 8μm the observed antibonding resonance strongly narrows. This can be explained as a Fano interference between the isolated slanted dimer antibonding resonance and the (1,0) Wood-Rayleigh (WR) anomaly. As has been explained in detail elsewhere,[1] two different interference regimes are observed depending on the relative spectral locations of the isolated dimer resonance (IDR) and of the WR anomaly. When the WR anomaly is on the high energy side of the isolated dimer resonance ($\lambda_{WR} < \lambda_{IDR}$), very little radiative coupling can occur as the allowed diffracted orders are all of higher energy than the plasmon resonance. In the other regime, $\lambda_{WR} > \lambda_{IDR}$, the radiative coupling is strong and a sharp and intense dip is produced in the long wavelength tail of the isolated dimer resonance[1]. This is

[1] Auguié, B.; Barnes, W. L. *Phys. Rev. Lett.* **2008**, *101*, 1–4.

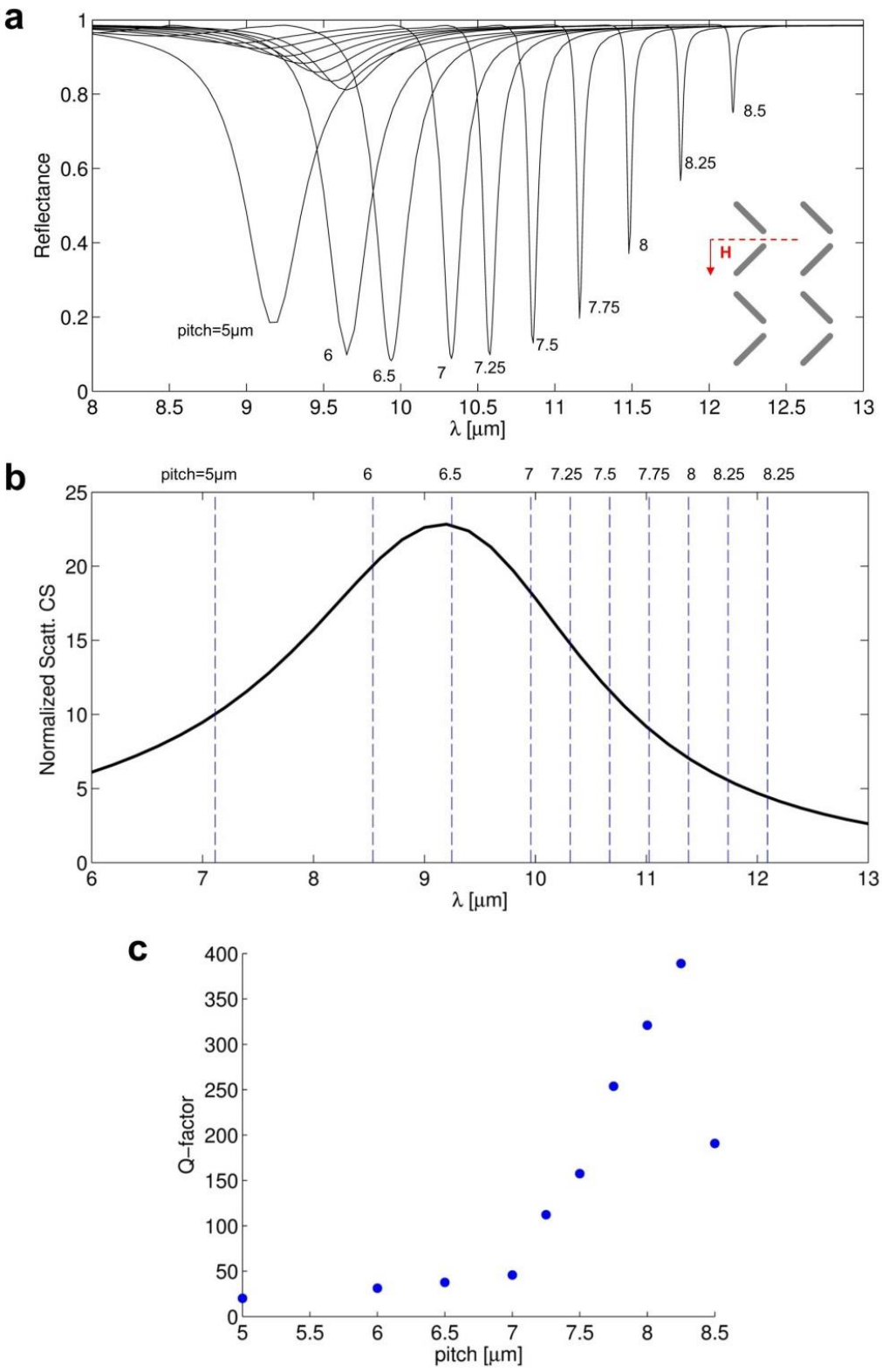

Figure S4. (a) Calculated reflectance spectra of the slanted dimer array depicted in the inset, for different array pitches. Geometrical parameters are α = 30°, β = 90°, h = 1.8μm, g = 100nm. TM-polarized light impinges at 25° along the scattering plane depicted in the inset; (b) Scattering cross section of the isolated slanted dimer; (c) Calculated quality factors for the reflectance dips shown in (a).

seen comparing the reflectance spectra of Figure S4a with the relative position of the (1,0) WR anomaly with respect to the insulated dimer antibonding resonance, Figure S4b. Figure S4c reports the calculated Quality factors (Q-factors) for the different pitches considered. These are calculated as $Q = \lambda_{dip}/\Delta\lambda$, being λ_{dip} the resonant wavelength and $\Delta\lambda$ the dip half width at half maximum. These parameters are calculated by lorentzian fits of portions of the reflectance curves close to the dips. A maximum Q of 389 is predicted for a pitch of 8.25μm.

5. Proof-of-concept molecule deposition on top of slanted nanorod dimers.

The possibility to produce an electric hot spot suspended in air, away from any substrate effects, is a particularly interesting feature of the presented slanted architecture, which can be exploited for IR sensing purposes. In order to provide a reliable sensing platform, however, the structure should be able to withstand the capillary forces and fluidic stresses involved in drying deposition processes. In addition, the possibility to successfully deposit molecules onto the rods terminations, where the field enhancement is highest, should be demonstrated.

We show here the results of two deposition tests of a fluorescent molecule on top of the slanted nanorods structures. Two different deposition processes were considered: critical point drying (CPD) and drop casting. The first process is suited for deposition of very thin layers while minimizing the surface tension forces, thus avoiding any mechanical perturbation of the structure. In this case we want to demonstrate that the adhesion of the thin fluorophore layer in the gap region successfully takes place. By contrast, the drop casting method usually produces strong surface tension forces which in some case result in a bending or collapse of the dimers. However, by carefully choosing the geometrical parameters of the dimer, we show that arrays of slanted rods can be fabricated which can withstand these strong mechanical stresses.

We prepared a sample of rods dimer with same geometrical characteristics as in Figure 1 in the main text. Then we deposited a fluorescent molecule, Brilliant Cresyl Blue (BCB), onto the sample

by immerging it into a solution with concentration 10μM. The BCB was dissolved in water and, after 1 hour of incubation, the solution was diluted with ethanol to avoid the collapse of the dimer, caused by surface tension of the water during the drying process. The sample was washed with clean ethanol and dried with CPD, performed with liquid carbon dioxide. With this technique the drying process does not cross the liquid-gas phase boundary, passing through the supercritical region, nullifying the surface tension. As a result, the fluorophore is deposited on the silver surfaces leaving the nanorod architecture intact (see Figure S5 inset).

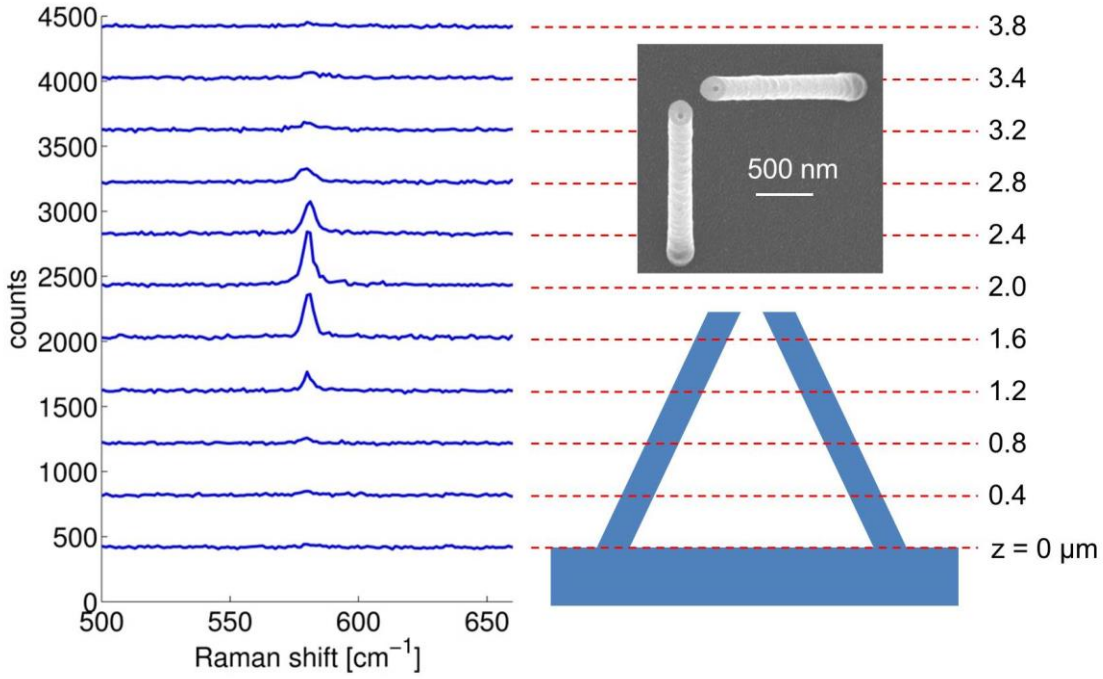

Figure S5. Raman spectra measured at different z-positions of the focus, as indicated in the side scheme. The spectra have been shifted by 400 counts from each other. The inset reports a SEM micrographs of a nanorod dimer after deposition of BCB.

In order to verify the adhesion of the fluorescent molecules in the gap region, we measured Raman spectra of the dried sample for different z-positions of the focal point (Figure S5). A Renishaw inVia Raman Microscope was used. The signal was acquired on a single nanorod dimer in reflection configuration with 0.5 seconds integration time and 0.025mW exciting laser source (633nm). As can be seen from the spectra, when the laser beam spans the top of the structure, the maximum of Raman signal is observed at k = 578 cm^{-1}, corresponding to a Raman transition of BCB.

This proves that a significant amount of fluorophore has been successfully deposited on rods terminations, where the electric field enhancement is expected to be higher.

Further deposition tests were performed using a standard drop casting procedure. As already mentioned, in this case the surface tension arising during the evaporation produces stronger intra dimer forces, especially at the rods terminations. These resulted in the collapse (namely, gap reduced to zero) of part of the rod arrays with heights exceeding 1μm. By contrast, smaller rods have proven to withstand the drying.

A sample has been fabricated with height of 930nm, angles $\alpha = 32°$ and $\beta = 180°$, gap 100nm and pitch 5μm. The geometrical parameters have been tuned in order to produce a bonding resonance at 6μm, close to BCB resonant mode assigned to NH2 scissors and asymmetric stretch of carbon rings (shaded peak in the measured absorbance spectrum of BCB, Figure S6a). A drop of BCB with concentration 1mM has been deposited onto the sample and subsequently has been let dry at room temperature. Figure S6b (inset) shows a SEM image of one dimer of the array after the deposition. As can be seen the structure morphology is intact, while a layer of fluorophore uniformly covers the all the metallic surfaces.

Infrared reflectance measurements have performed on the sample before and after deposition by micro-FITR spectroscopy, on a range between 3 and 7μm. The aperture is fixed to 45μm x 45μm. The light passes through a Cassegrain objective with 0.58 numerical aperture, 15x magnification, 20-30 degrees impinging angle. The obtained spectra are reported in Figure S6b. Three dips can be observed. As can be easily verified by simulations (not shown), the first dip ($\lambda = 4.3$ μm) is associated with the antibonding resonance of the isolated dimer, the second is a Fano resonance produced by the (1,0) Wood-Rayleigh anomaly and the third is the fundamental bonding resonance of the structure. We notice that, after the deposition (red curve), the bonding resonance still can be observed, proving that the gap remained opened and the collapse did not take place. A clear sign of the molecule IR spectrum can be recognised in the appearance of a small local reflectance peak

superimposed to the bonding resonance, which spectrally matches the aforementioned resonance of BCB.

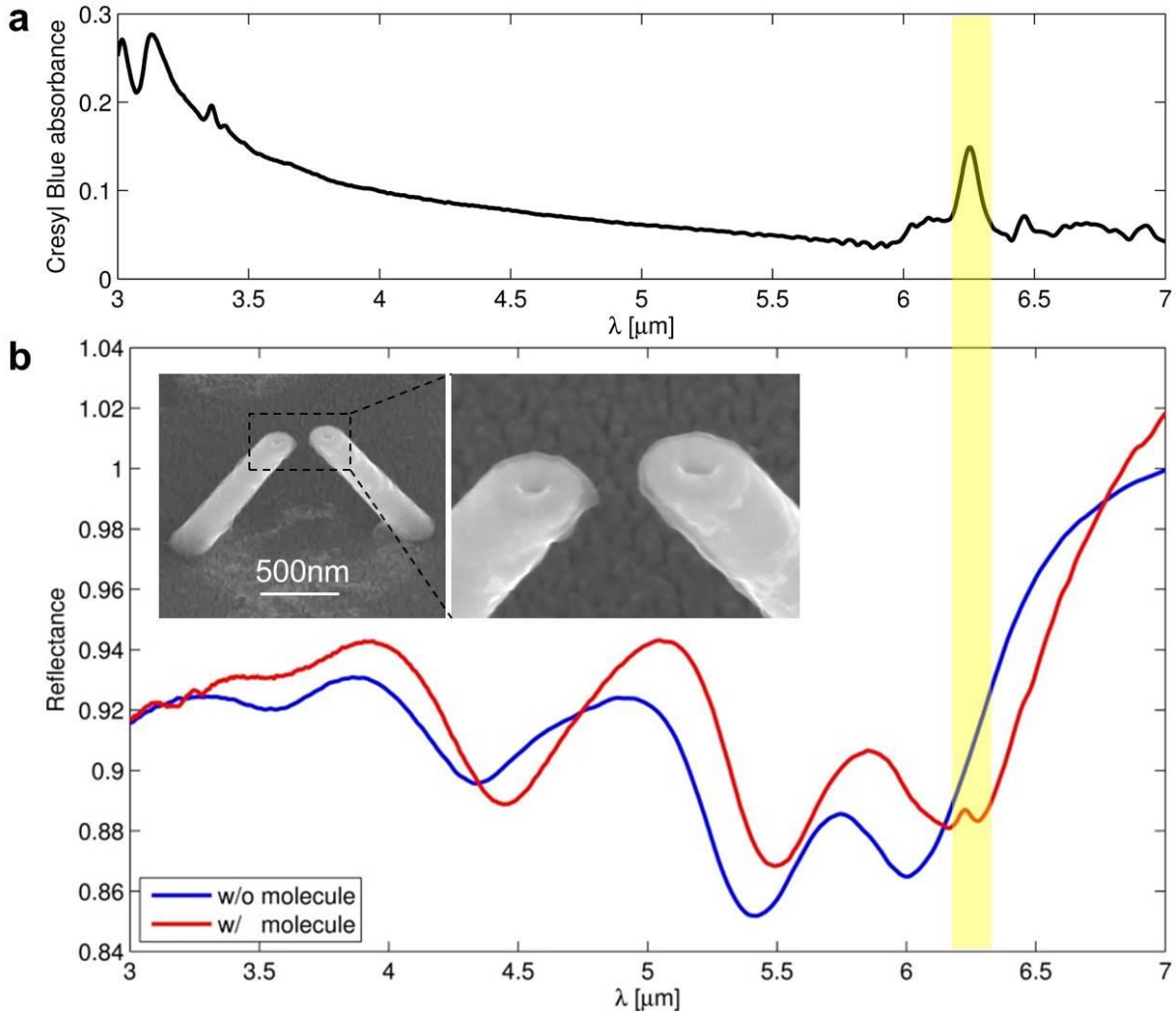

Figure S6. Above: measured IR spectrum of bulk BCB fluorophore. Below: FTIR reflectance spectra measured before (blue line) and after (red line) deposition of BCB on top of a nanorod dimer array (height 930nm, α = 32°, β = 180°, gap 100nm, pitch 5μm). The insets report SEM images of one dimer of the array after deposition.